

## Strategy towards the extraction of the Sivers function with transverse momentum dependent evolution

M. Anselmino,<sup>1,2</sup> M. Boglione,<sup>1,2</sup> and S. Melis<sup>3</sup>

<sup>1</sup>*Dipartimento di Fisica Teorica, Università di Torino, Via P. Giuria 1, I-10125 Torino, Italy*

<sup>2</sup>*INFN, Sezione di Torino, Via P. Giuria 1, I-10125 Torino, Italy*

<sup>3</sup>*European Centre for Theoretical Studies in Nuclear Physics and Related Areas (ECT\*), Villa Tambosi, Strada delle Tabarelle 286, I-38123 Villazzano, Trento, Italy*

(Received 12 April 2012; published 26 July 2012)

The QCD evolution of the unpolarized transverse momentum dependent (TMD) distribution functions and of the Sivers functions have been discussed in recent papers. Following such results we reconsider previous extractions of the Sivers functions from semi-inclusive deep inelastic scattering data and propose a simple strategy which allows to take into account the  $Q^2$  dependence of the TMDs in comparison with experimental findings. A clear evidence of the phenomenological success of the TMD-evolution equations is given, mostly, by the newest COMPASS data off a transversely polarized proton target.

DOI: [10.1103/PhysRevD.86.014028](https://doi.org/10.1103/PhysRevD.86.014028)

PACS numbers: 13.60.-r, 13.85.Ni, 13.88.+e

### I. INTRODUCTION AND FORMALISM

The exploration of the three-dimensional structure of the nucleons, both in momentum and configuration space, is one of the major issues in hadron high-energy physics, with dedicated experimental and theoretical efforts. In particular, several semi-inclusive deep inelastic scattering (SIDIS) experiments are either running or being planned. From the measurements of azimuthal asymmetries, both with unpolarized and polarized nucleons, one obtains information on the transverse momentum dependent parton distribution functions (TMD PDFs) and on the transverse momentum dependent fragmentation functions (TMD FFs). The TMD PDFs and the TMD FFs are often globally referred to simply as TMDs. The TMD PDFs convey information on the momentum distributions of partons inside protons and neutrons.

The analysis of the experimental data is based on the so-called TMD factorization, which links measurable cross sections and spin asymmetries to a convolution of TMDs. In particular, the Sivers function, which describes the number density of unpolarized quarks inside a transversely polarized proton, has received much attention and has been extracted from SIDIS data by several groups, with consistent results [1–6]. However, all these phenomenological fits of the Sivers function (and other TMDs) have been performed so far using a simplified version of the TMD factorization scheme, in which the QCD scale dependence of the TMDs—which was unknown—is either neglected or limited to the collinear part of the unpolarized PDFs. While this might not be a serious numerical problem when considering only experimental data which cover limited ranges of low  $Q^2$  values, it is not correct in principle, and taking into account the appropriate  $Q^2$  evolution might be numerically relevant for predictions at higher  $Q^2$  values, like future electron-ion or electron-nucleon colliders and Drell-Yan experiments.

Recently, the issue of the QCD evolution of unpolarized TMDs and of the Sivers function has been studied in a series of papers [7–9] and a complete TMD factorization framework is now available for a consistent treatment of SIDIS data and the extraction of TMDs. A first application of the new TMD-evolution equations to some limited samples of the HERMES and COMPASS data [10] has indeed shown clear signs of the  $Q^2$  TMD evolution.

We follow here Refs. [8,9] adopting their formalism, which includes the explicit  $Q^2$  dependence of the TMDs, and apply it to the extraction of the Sivers function from SIDIS data, exploiting the latest HERMES [11] and COMPASS [12] results. In the remainder of this section we present the explicit formalism: in Subsection IA we describe the setup and structure of the TMD-evolution equations, in Subsection IB we discuss the parametrizations used for the unknown input functions, while in Sec. IC we present analytical solutions of the TMD-evolution equations obtained under a specific approximation.

In Sec. II we perform a best fit of the SIDIS Sivers asymmetries, taking into account the different  $Q^2$  values of each data point and the  $Q^2$  dependence of the TMDs; we compare our results with a similar analysis performed without the TMD evolution. Differences between Sivers functions extracted from data with and without the TMD evolution are shown and commented. In all this we differ from Ref. [10], which explicitly shows the evolution of an existing fit of the Sivers SIDIS asymmetry [13] from the average value  $\langle Q^2 \rangle = 2.4 \text{ GeV}^2$  for HERMES data [11] to the average value of  $\langle Q^2 \rangle = 3.8 \text{ GeV}^2$  for the most recent COMPASS data [12]. Further comments and conclusions are given in Sec. III.

#### A. Formalism for transverse momentum dependent $Q^2$ dependence

In Refs. [7,8], Collins, Aybat and Rogers have proposed a scheme to describe the  $Q^2$  evolution of the TMD

unpolarized distribution and fragmentation functions: within the framework of the Collins-Soper-Sterman factorization formalism [14,15], they can describe the nonperturbative, low-transverse momentum region and, at the same time, consistently include the perturbative corrections affecting the region of larger energies and momentum transfers. However, this formalism cannot be directly applied to spin-dependent distribution functions, like the Siverson function [16], for which the collinear limit does not exist.

More recently, an extension of the unpolarized TMD-evolution formalism was presented in Ref. [9] to provide a framework in which also spin-correlated PDFs can be accounted for. For our purposes, we will use Eq. (44) of Ref. [9] which, compared to the unpolarized TMD-evolution scheme, Eq. (26) of Ref. [8], requires the extra aid of a phenomenological input function embedding the missing information on the evolved function, that, in the case of the Siverson function, is both of perturbative and nonperturbative nature. Although the unpolarized PDF and FF TMD-evolution equations are in principle known [8], in this paper we adopt the simplified functional form of the evolution equation, as proposed for the Siverson function in Ref. [9], for all TMD functions, for consistency.

Thus, we strictly follow Ref. [9] and combine their Eqs. (44), (43) and (30), taking, as suggested [9], the renormalization scale  $\mu^2$  and the regulating parameters  $\zeta_F$  and  $\zeta_D$  all equal to  $Q^2$ . Then, the QCD evolution of the TMDs in the coordinate space can be written as

$$\begin{aligned} \tilde{F}(x, \mathbf{b}_T; Q) &= \tilde{F}(x, \mathbf{b}_T; Q_0) \\ &\times \exp\left\{\ln\frac{Q}{Q_0}\tilde{K}(b_T; Q_0) + \int_{Q_0}^Q \frac{d\mu}{\mu} \gamma_F\left(\mu, \frac{Q^2}{\mu^2}\right)\right\}, \end{aligned} \quad (1)$$

where  $\tilde{F}$  can be either the unpolarized parton distribution,  $\tilde{F}(x, \mathbf{b}_T; Q) = \tilde{f}_{q/p}(x, \mathbf{b}_T; Q)$ , the unpolarized fragmentation function  $\tilde{F}(x, \mathbf{b}_T; Q) = \tilde{D}_{h/q}(z, \mathbf{b}_T; Q)$ , or the first derivative, with respect to the parton impact parameter  $b_T$ , of the Siverson function,  $\tilde{F}(x, \mathbf{b}_T; Q) = \tilde{f}_{1T}^{\perp f}(x, \mathbf{b}_T; Q)$ . Notice that throughout the paper  $b_T$ -dependent distribution and fragmentation functions will be denoted with a  $\sim$  on top.

In the above equation the function  $\tilde{K}$  is given in general by [9]

$$\tilde{K}(b_T, \mu) = \tilde{K}(b_*, \mu_b) + \left[ \int_{\mu}^{\mu_b} \frac{d\mu'}{\mu'} \gamma_K(\mu') \right] - g_K(b_T), \quad (2)$$

with, at  $\mathcal{O}(\alpha_s)$  [14,15],

$$\tilde{K}(b_*, \mu_b) = -\frac{\alpha_s C_F}{\pi} [\ln(b_*^2 \mu_b^2) - \ln 4 + 2\gamma_E] \quad (3)$$

$$b_*(b_T) \equiv \frac{b_T}{\sqrt{1 + b_T^2/b_{\max}^2}} \quad \mu_b = \frac{C_1}{b_*(b_T)}. \quad (4)$$

The first two terms in Eq. (2) are perturbative and depend on the scale  $\mu$  through the coupling  $\alpha_s(\mu)$ , while the last term is nonperturbative, but scale-independent.  $C_1$  is a constant parameter that can be fixed to optimize the perturbative expansion, as explained in Ref. [15]. References [8,9] adopt the particular choice  $C_1 = 2e^{-\gamma_E}$  which automatically implies  $\tilde{K}(b_*, \mu_b) = 0$ , considerably simplifying the  $b_T$  dependence of the Collins-Soper-Sterman kernel  $\tilde{K}(b_T, \mu)$ , Eq. (2).

The anomalous dimensions  $\gamma_F$  and  $\gamma_K$  appearing respectively in Eqs. (1) and (2), are given, again at order  $\mathcal{O}(\alpha_s)$ , by [8,15]

$$\begin{aligned} \gamma_F\left(\mu; \frac{Q^2}{\mu^2}\right) &= \alpha_s(\mu) \frac{C_F}{\pi} \left(\frac{3}{2} - \ln\frac{Q^2}{\mu^2}\right) \\ \gamma_K(\mu) &= \alpha_s(\mu) \frac{2C_F}{\pi}. \end{aligned} \quad (5)$$

By making use of Eqs. (2)–(5), the evolution of  $\tilde{F}(x, \mathbf{b}_T; Q)$  in Eq. (1) can then be written as

$$\tilde{F}(x, \mathbf{b}_T; Q) = \tilde{F}(x, \mathbf{b}_T; Q_0) \tilde{R}(Q, Q_0, b_T) \exp\left\{-g_K(b_T) \ln\frac{Q}{Q_0}\right\}, \quad (6)$$

with

$$\begin{aligned} \tilde{R}(Q, Q_0, b_T) & \\ &\equiv \exp\left\{\ln\frac{Q}{Q_0} \int_{Q_0}^{\mu_b} \frac{d\mu'}{\mu'} \gamma_K(\mu') + \int_{Q_0}^Q \frac{d\mu}{\mu} \gamma_F\left(\mu, \frac{Q^2}{\mu^2}\right)\right\}. \end{aligned} \quad (7)$$

The  $Q^2$  evolution is driven by the functions  $g_K(b_T)$  and  $\tilde{R}(Q, Q_0, b_T)$ . While the latter, Eq. (7), can be easily evaluated, numerically or even analytically, the former is essentially unknown and will need to be taken from independent experimental inputs.

The explicit expression of the TMDs in the momentum space, with the QCD  $Q^2$  dependence, can be obtained by Fourier-transforming Eq. (6), obtaining [9]

$$\hat{f}_{q/p}(x, k_{\perp}; Q) = \frac{1}{2\pi} \int_0^{\infty} db_T b_T J_0(k_{\perp} b_T) \tilde{f}_{q/p}(x, b_T; Q) \quad (8)$$

$$\hat{D}_{h/q}(z, p_{\perp}; Q) = \frac{1}{2\pi} \int_0^{\infty} db_T b_T J_0(k_T b_T) \tilde{D}_{h/q}(z, b_T; Q) \quad (9)$$

$$\hat{f}_{1T}^{\perp f}(x, k_{\perp}; Q) = \frac{-1}{2\pi k_{\perp}} \int_0^{\infty} db_T b_T J_1(k_{\perp} b_T) \tilde{f}_{1T}^{\perp f}(x, b_T; Q), \quad (10)$$

where  $J_0$  and  $J_1$  are Bessel functions. In this paper we denote the distribution and fragmentation functions which depend on the transverse momenta (TMDs) with a ‘‘wide hat’’ on top.  $\hat{f}_{q/p}$  is the unpolarized TMD distribution function for a parton of flavor  $q$  inside a proton, and  $\hat{D}_{h/q}$  is the unpolarized TMD fragmentation function for hadron  $h$  inside a parton  $q$ .  $\hat{f}_{1T}^{\perp q}$  is the Sivers distribution defined, for unpolarized partons inside a transversely polarized proton, as

$$\hat{f}_{q/p^i}(x, \mathbf{k}_\perp, \mathbf{S}; Q) = \hat{f}_{q/p}(x, k_\perp; Q) - \hat{f}_{1T}^{\perp q}(x, k_\perp; Q) \frac{\epsilon_{ij} k_\perp^i S^j}{M_p} \quad (11)$$

$$= \hat{f}_{q/p}(x, k_\perp; Q) + \frac{1}{2} \Delta^N \hat{f}_{q/p^i}(x, k_\perp; Q) \frac{\epsilon_{ij} k_\perp^i S^j}{k_\perp}. \quad (12)$$

In our notation  $\mathbf{k}_\perp$  is the transverse momentum of the parton with respect to the parent nucleon direction and  $\mathbf{p}_\perp$  is the transverse momentum of the final hadron with respect to the parent parton direction. Notice that in Refs. [8,9] all transverse momenta are defined in a unique frame, the so-called hadron frame, in which the measured hadrons have zero transverse momentum. In this frame, the initial and the final parton transverse momenta are denoted, respectively, by  $\mathbf{k}_{1T}$  and  $\mathbf{k}_{2T}$ . They are related to our notation by:  $\mathbf{k}_\perp = \mathbf{k}_{1T}$  and, at leading order in  $p_\perp$ ,  $\mathbf{p}_\perp = -z\mathbf{k}_{2T}$ . This requires some attention when dealing with the fragmentation functions. Usually, the TMD FFs are defined in terms of the *hadronic*  $p_\perp$ , i.e., the transverse momentum of the final hadron  $h$  with respect to the direction of the fragmenting parton  $q$ , while, following Refs. [8,9], the Fourier transform (9) is performed from the impact parameter space of the fragmenting parton ( $b_T$ ) into the corresponding *partonic* transverse momentum ( $\mathbf{k}_T = \mathbf{p}_\perp/z$ ) in the hadron frame. This will generate some extra  $z^2$  factors, as explained in detail in Sec. IB.

## B. Parametrization of unknown functions

Equations (8)–(10) can be adopted as the appropriate functional forms, with the correct  $Q^2$  dependence induced by Eqs. (6) and (7), to be used in the extraction of phenomenological information on the unpolarized and Sivers TMDs. In order to do so, one should start with a parametrization of the unknown functions inside Eq. (6):  $g_K(b_T)$  and  $\tilde{F}(x, b_T; Q_0)$ . As already anticipated,  $g_K(b_T)$  is a non-perturbative, but universal function, which in the literature is usually parametrized in a quadratic form. As in Refs. [9,10], we will adopt the results provided by a recent fit of Drell-Yan data [17], and assume

$$g_K(b_T) = \frac{1}{2} g_2 b_T^2 \quad \text{with} \quad g_2 = 0.68 \text{ GeV}^2 \quad (13)$$

corresponding to  $b_{\max} = 0.5 \text{ GeV}^{-1}$ .

We should now parametrize the function  $\tilde{F}(x, b_T; Q_0)$  in configuration space. We wish to test the effect of the TMD evolution in the extraction of the Sivers functions from data; in particular, we will compare the extraction based on TMD evolution with previous extractions which did not take such an evolution into account. Then, we parametrize the input function  $\tilde{F}(x, b_T; Q_0)$  by requiring that its Fourier transform, which gives the corresponding TMD function in the transverse momentum space, coincides with the previously adopted  $k_\perp$ -Gaussian form, with the  $x$  dependence factorized out. That was also done in Refs. [8,9], assuming for the unpolarized TMD PDF

$$\tilde{f}_{q/p}(x, b_T; Q_0) = f_{q/p}(x, Q_0) \exp\{-\alpha^2 b_T^2\}, \quad (14)$$

where  $f_{q/p}(x, Q_0)$  is the usual integrated PDF of parton  $q$  inside proton  $p$ , evaluated at  $Q_0$ ; the value of  $\alpha^2$  is fixed by requiring the desired behavior of the distribution function in the transverse momentum space at the initial scale  $Q_0$ : taking  $\alpha^2 = \langle k_\perp^2 \rangle / 4$  one recovers

$$\hat{f}_{q/p}(x, k_\perp; Q_0) = f_{q/p}(x, Q_0) \frac{1}{\pi \langle k_\perp^2 \rangle} e^{-k_\perp^2 / \langle k_\perp^2 \rangle}, \quad (15)$$

in agreement with Refs. [5,13,18].

Similar relations hold for the TMD FFs, with an additional  $z^2$  factor due to the fact that the Fourier transform (9) leads from the impact parameter space of the fragmenting parton in the hadron frame to the corresponding partonic transverse momentum  $\mathbf{k}_T$ , while the TMD FFs are functions of the transverse momentum  $\mathbf{p}_\perp = z\mathbf{k}_T$  of the final hadron with respect to the fragmenting parton direction. This requires the initial parametrization

$$\tilde{D}_{h/q}(z, b_T; Q_0) = \frac{1}{z^2} D_{h/q}(z, Q_0) \exp\{-\beta^2 b_T^2\}, \quad (16)$$

where  $D_{h/q}(z, Q_0)$  is the usual integrated FF evaluated at the initial scale  $Q_0$ , and  $\beta^2 = \langle p_\perp^2 \rangle / 4z^2$  in order to recover the previously adopted behavior [5,13,18] of the fragmentation function in the  $p_\perp$  transverse momentum space at  $Q_0$

$$\hat{D}_{h/q}(z, p_\perp; Q_0) = D_{h/q}(z, Q_0) \frac{1}{\pi \langle p_\perp^2 \rangle} e^{-p_\perp^2 / \langle p_\perp^2 \rangle}. \quad (17)$$

Analogously, we parametrize the Sivers function at the initial scale  $Q_0$  as

$$\tilde{f}_{1T}^\perp(x, b_T; Q_0) = -2\gamma^2 f_{1T}^\perp(x; Q_0) b_T e^{-\gamma^2 b_T^2}, \quad (18)$$

which, when Fourier-transformed according to Eq. (10), yields

$$\hat{f}_{1T}^\perp(x, k_\perp; Q_0) = f_{1T}^\perp(x; Q_0) \frac{1}{4\pi\gamma^2} e^{-k_\perp^2 / 4\gamma^2}. \quad (19)$$

Equation (19) agrees with our previous parametrization of the Sivers function, at the initial scale  $Q_0$  [5,13,18], taking

$$4\gamma^2 \equiv \langle k_{\perp}^2 \rangle_S = \frac{M_1^2 \langle k_{\perp}^2 \rangle}{M_1^2 + \langle k_{\perp}^2 \rangle} \quad (20)$$

$$f_{1T}^{\perp}(x; Q_0) = -\frac{M_p}{2M_1} \sqrt{2e} \Delta^N f_{q/p^i}(x, Q_0) \frac{\langle k_{\perp}^2 \rangle_S}{\langle k_{\perp}^2 \rangle}. \quad (21)$$

$M_1$  is a mass parameter,  $M_p$  the proton mass and  $\Delta^N f_{q/p^i}(x, Q_0)$  is the  $x$ -dependent term of the Siverts function, evaluated at the initial scale  $Q_0$  and written as [5,13,18]

$$\Delta^N f_{q/p^i}(x, Q_0) = 2\mathcal{N}_q(x) f_{q/p}(x, Q_0), \quad (22)$$

where  $\mathcal{N}_q(x)$  is a function of  $x$ , properly parametrized (we will come back to details of the Siverts function parametrization in Sec. II).

The final evolution equations of the unpolarized TMD PDFs and TMD FFs, in the configuration space, are obtained inserting Eqs. (14) and (16) into Eq. (6)

$$\begin{aligned} \tilde{f}_{q/p}(x, b_T; Q) &= f_{q/p}(x, Q_0) \tilde{R}(Q, Q_0, b_T) \\ &\times \exp\left\{-b_T^2 \left(\alpha^2 + \frac{g_2}{2} \ln \frac{Q}{Q_0}\right)\right\} \end{aligned} \quad (23)$$

$$\begin{aligned} \tilde{D}_{h/q}(z, b_T; Q) &= \frac{1}{z^2} D_{h/q}(z, Q_0) \tilde{R}(Q, Q_0, b_T) \\ &\times \exp\left\{-b_T^2 \left(\beta^2 + \frac{g_2}{2} \ln \frac{Q}{Q_0}\right)\right\}, \end{aligned} \quad (24)$$

with  $\alpha^2 = \langle k_{\perp}^2 \rangle / 4$ ,  $\beta^2 = \langle p_{\perp}^2 \rangle / (4z^2)$ ,  $g_2$  given in Eq. (13) and  $\tilde{R}(Q, Q_0, b_T)$  in Eq. (7).

The evolution of the Siverts function is obtained through its first derivative, inserting Eq. (18) into Eq. (6)

$$\begin{aligned} \tilde{f}_{1T}^{\perp}(x, b_T; Q) &= -2\gamma^2 f_{1T}^{\perp}(x; Q_0) \tilde{R}(Q, Q_0, b_T) b_T \\ &\times \exp\left\{-b_T^2 \left(\gamma^2 + \frac{g_2}{2} \ln \frac{Q}{Q_0}\right)\right\} \end{aligned} \quad (25)$$

with  $\gamma^2$  and  $f_{1T}^{\perp}(x; Q_0)$  given in Eqs. (20)–(22).

Equations (23)–(25) show that the  $Q^2$  evolution is controlled by the logarithmic  $Q$  dependence of the  $b_T$  Gaussian width, together with the factor  $\tilde{R}(Q, Q_0, b_T)$ : for increasing values of  $Q^2$ , they are responsible for the typical broadening effect already observed in Refs. [8,9].

It is important to stress that although the structure of Eq. (1) is general and holds over the whole range of  $b_T$  values, the input function  $\tilde{F}(x, \mathbf{b}_T, Q_0)$  is only designed to work in the large- $b_T$  region, corresponding to low  $k_{\perp}$  values. Therefore, this formalism is perfectly suitable for phenomenological applications in the kinematical region we are interested in, but the parametrization of the input function should be revised in the case one wishes to apply it to a wider range of transverse momenta, like higher  $Q^2$  processes where perturbative corrections become important.

### C. Analytical solution of the TMD evolution equations

The TMD evolution in Eqs. (23)–(25) implies, apart from the explicit Gaussian dependence, a further nontrivial dependence on the parton impact parameter  $b_T$  through the evolution kernel  $\tilde{R}(Q, Q_0, b_T)$  and the upper integration limit  $\mu_b$ , Eq. (4), which appears in Eq. (7); consequently, it needs to be evaluated numerically. However, the evolution equations can be solved analytically by making a simple approximation on this  $b_T$  dependence. A close examination of Eq. (4) shows that  $\mu_b$  is a decreasing function of  $b_T$  that very rapidly freezes to the constant value  $C_1/b_{\max} = \mu_b(b_T \rightarrow \infty)$ : more precisely, the approximation  $\mu_b = \text{const}$  holds for any  $b_T \gtrsim 1 \text{ GeV}^{-1}$ . As very small values of  $b_T$  correspond to very large values of  $k_{\perp}$ , this approximation is safe in our framework, where the typical  $k_{\perp}$  are less than 1 GeV. Neglecting the  $b_T$  dependence of  $\mu_b$ , the factor  $\tilde{R}(Q, Q_0, b_T)$  does not depend on  $b_T$  anymore, see Eq. (7), and can even be integrated analytically by using an explicit representation of  $\alpha_s(Q)$ . Hereafter we will refer to it as  $R(Q, Q_0)$ , with  $R(Q, Q_0) \equiv \tilde{R}(Q, Q_0, b_T \rightarrow \infty)$ . Fig. 1 shows the evolution factor  $\tilde{R}(Q, Q_0, b_T)$  plotted as a function of  $b_T$  at two fixed values

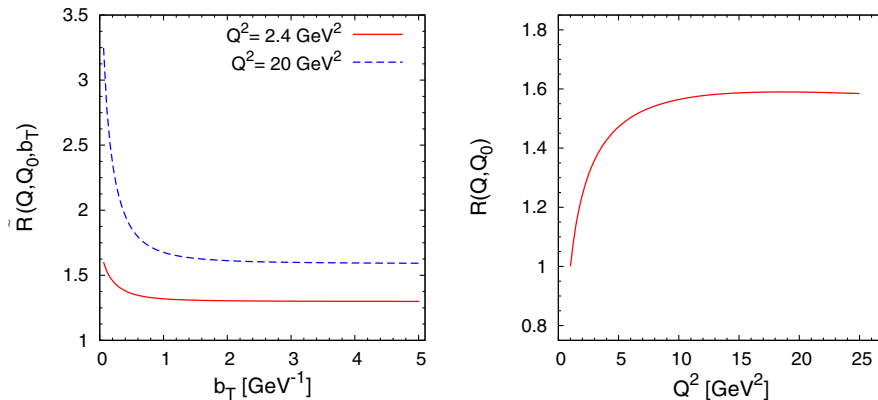


FIG. 1 (color online). In the left panel, the evolution factor  $R(Q, Q_0, b_T)$  is plotted as a function of  $b_T$  at two fixed values of  $Q^2$ . In the right panel we show  $R(Q, Q_0) \equiv R(Q, Q_0, b_T \rightarrow \infty)$  as a function of  $Q^2$ . In both cases,  $Q_0^2 = 1 \text{ GeV}^2$ .

of  $Q^2$  (left panel), and  $R(Q, Q_0)$  as a function of  $Q^2$  (right panel). It is clear that  $R(Q, Q_0)$  settles to a constant value for  $b_T \gtrsim 1 \text{ GeV}^{-1}$ . In both cases,  $Q_0^2 = 1 \text{ GeV}^2$ . Small  $b_T$  values, for which this approximation loses its validity, do not contribute much to the Fourier transforms (8)–(10), as it will be shown explicitly in our results (see Fig. 2). Such an analytical solution is anyway of great help as it provides a simple illustration of all the main features of the TMD evolution.

Thus, in this approximation, the TMD-evolution Eq. (6) only depends on  $b_T$  through the nonperturbative function  $g_K(b_T)$ , which has been chosen to be a quadratic function of  $b_T$ , Eq. (13), and through the  $b_T$  dependence of the initial input function  $\tilde{F}(x, \mathbf{b}_T; Q_0)$  which has been chosen to be Gaussian. It results in a  $b_T$ -Gaussian form, with a width which depends logarithmically on  $Q/Q_0$ , for the TMD-evolution equation. For the unpolarized TMD PDFs one has

$$\tilde{f}_{q/p}(x, \mathbf{b}_T; Q) = f_{q/p}(x, Q_0)R(Q, Q_0) \times \exp\left[-\frac{b_T^2}{4}\left(\langle k_\perp^2 \rangle + 2g_2 \ln \frac{Q}{Q_0}\right)\right]. \quad (26)$$

Its Fourier transform, Eq. (8), delivers a Gaussian distribution in the transverse momentum space as well

$$\hat{f}_{q/p}(x, k_\perp; Q) = f_{q/p}(x, Q_0)R(Q, Q_0) \frac{e^{-k_\perp^2/w^2}}{\pi w^2}, \quad (27)$$

where  $f_{q/p}(x, Q_0)$  is the usual integrated PDF evaluated at the initial scale  $Q_0$  and, most importantly,  $w^2 \equiv w^2(Q, Q_0)$  is the ‘‘evolving’’ Gaussian width, defined as

$$w^2(Q, Q_0) = \langle k_\perp^2 \rangle + 2g_2 \ln \frac{Q}{Q_0}. \quad (28)$$

It is worth noticing that the  $Q^2$  evolution of the TMD PDFs is now determined by the overall factor  $R(Q, Q_0)$  and, most crucially, by the  $Q^2$ -dependent Gaussian width  $w(Q, Q_0)$ .

The TMD FFs evolve in a similar way, Eq. (24),

$$\tilde{D}_{h/q}(z, b_T; Q) = \frac{1}{z^2} D_{h/q}(z, Q_0) R(Q, Q_0) \times \exp\left[-\frac{b_T^2}{4z^2}\left(\langle p_\perp^2 \rangle + 2z^2 g_2 \ln \frac{Q}{Q_0}\right)\right], \quad (29)$$

leading to the TMD FF in momentum space

$$\hat{D}_{h/q}(z, p_\perp; Q) = D_{h/q}(z, Q_0) R(Q, Q_0) \frac{e^{-p_\perp^2/w_F^2}}{\pi w_F^2}, \quad (30)$$

with an evolving and  $z$ -dependent Gaussian width  $w_F \equiv w_F(Q, Q_0)$  given by

$$w_F^2 \equiv w_F^2(Q, Q_0) = \langle p_\perp^2 \rangle + 2z^2 g_2 \ln \frac{Q}{Q_0}. \quad (31)$$

For the Sivers distribution function, by Fourier-transforming Eq. (25) (with  $\tilde{R} \rightarrow R$ ) as prescribed by Eq. (10), we obtain [see also Eqs. (11), (12), (20), and (21)]:

$$\Delta^N \hat{f}_{q/p^i}(x, k_\perp; Q) = \frac{k_\perp}{M_1} \sqrt{2} e^{-\frac{\langle k_\perp^2 \rangle_S}{\langle k_\perp^2 \rangle}} \Delta^N f_{q/p^i}(x, Q_0) R(Q, Q_0) \frac{e^{-k_\perp^2/w_S^2}}{\pi w_S^4}, \quad (32)$$

with

$$w_S^2(Q, Q_0) = \langle k_\perp^2 \rangle_S + 2g_2 \ln \frac{Q}{Q_0}. \quad (33)$$

It is interesting to notice that the evolution factor  $R(Q, Q_0)$ , controlling the TMD evolution according to Eqs. (27), (30), and (32) is the same for all

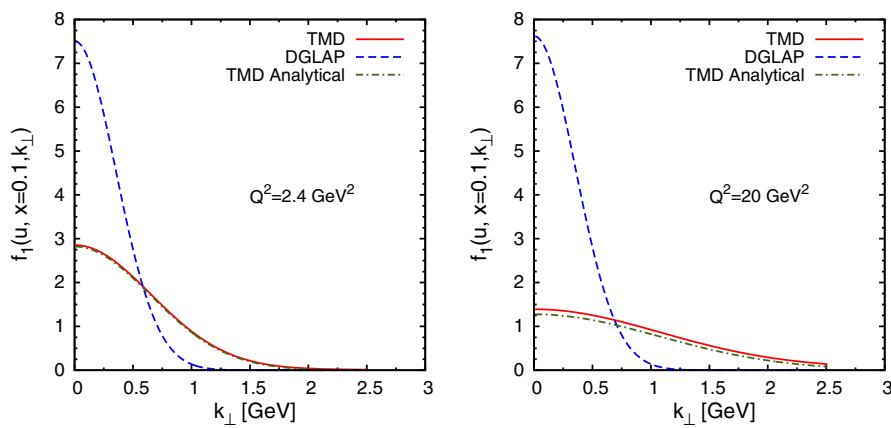


FIG. 2 (color online). The left panel shows the unpolarized TMD PDF,  $\hat{f}_{u/p}$ , evolved from the initial scale,  $Q_0^2 = 1 \text{ GeV}^2$ , to  $Q^2 = 2.4 \text{ GeV}^2$ , using TMD evolution (red, solid line), DGLAP evolution (blue, dashed line) and the analytical approximated TMD evolution (green, dot-dashed line). The right panel shows the same functions at the scale  $Q^2 = 20 \text{ GeV}^2$ . Notice that, while there is hardly any difference between the DGLAP-evolved lines at  $Q^2 = 2.4$  and  $Q^2 = 20 \text{ GeV}^2$ , the TMD evolution induces a fast decrease in size of the TMD PDF functions at large  $Q^2$  and a simultaneous widening of its Gaussian width. Here the analytical approximated evolution gives results in good agreement with the exact calculation even at large  $Q^2$  and  $k_\perp$ .

functions (TMD PDFs, TMD FFs and Sivers) and is flavor-independent; consequently it will appear, squared, in both numerator and denominator of the Sivers azimuthal asymmetry and, approximately, cancel out. Therefore, we can safely conclude that most of the TMD evolution of azimuthal asymmetries is controlled by the logarithmic  $Q$  dependence of the  $k_{\perp}$  Gaussian widths  $w^2(Q, Q_0)$ , Eqs. (28), (31), and (33). We will come back to this in Sec. II.

To illustrate the features of this new TMD-evolution, we compare it with the results obtained evolving only the collinear part,  $f_{q/p}(x, Q)$ , of the unpolarized TMD PDF according to the usual Dokshitzer-Gribov-Lipatov-Altarelli-Parisi (DGLAP) equations and assuming the  $k_{\perp}$ -dependent term of this function to be unaffected by evolution. In the left panel of Fig. 2 we show the  $k_{\perp}$  behavior of the unpolarized TMD PDF  $\hat{f}_{u/p}(x, k_{\perp}, Q^2)$ , at the fixed value  $x = 0.1$ , evaluated at the scale  $Q^2 = 2.4 \text{ GeV}^2$  (the average  $Q^2$  value for the HERMES experiment). In the right panel we show the same function at a higher scale,  $Q^2 = 20 \text{ GeV}^2$  (which is the highest bin average  $Q^2$  detected in the COMPASS experiment). In both cases the chosen initial scale is  $Q_0^2 = 1 \text{ GeV}^2$ . The red, solid line corresponds to the  $k_{\perp}$  distribution of the TMD PDF found by using the TMD evolution of Eq. (23) while the blue, dashed line represents the result obtained by using DGLAP evolution equations. At the initial scale,  $Q_0^2 = 1 \text{ GeV}^2$ , solid and dashed curves coincide, by definition. However, while the DGLAP evolution is so slow that there is hardly any difference between the DGLAP-evolved lines at  $Q^2 = 2.4 \text{ GeV}^2$  and  $Q^2 = 20 \text{ GeV}^2$ , the TMD evolution induces a fast decrease of the maximum values of the TMD PDF function with growing  $Q^2$ , and a simultaneous broadening of its Gaussian width, as observed in Refs. [8,9]. It is interesting to notice that the approximated evolution of Eq. (27),

corresponding to the green, dot-dashed line works really well, even for large  $Q^2$  values.

A similar study is performed in Fig. 3 for the Sivers function. Here, by DGLAP evolution we mean that the Sivers function evolves like an unpolarized collinear PDF, only through the factor  $f_{q/p}(x, Q)$  contained in its parametrization, Eq. (22). The parameters used for the plots are those given in Sec. II, although any set of realistic parameters would lead to the same conclusions. The left panel shows the ratio between the Sivers function and the TMD PDF,  $\Delta^N \hat{f}_{u/p^i}(x, k_{\perp}; Q)/(2\hat{f}_{u/p}(x, k_{\perp}; Q))$ , evaluated at the scale  $Q^2 = 2.4 \text{ GeV}^2$ . Again, the red, solid line is obtained using the TMD evolution of Eqs. (23) and (25), while the blue, dashed line is given by the DGLAP evolution. The green, dot-dashed line represents the results obtained using the approximated analytical TMD evolution of Eqs. (27) and (32). The right panel shows the same functions at the scale  $Q^2 = 20 \text{ GeV}^2$ . Similarly to the case of TMD PDFs, while there is no difference between the DGLAP-evolved lines at  $Q^2 = 2.4$  and  $Q^2 = 20 \text{ GeV}^2$ , the TMD evolution induces a fast decrease in the size of the TMD Sivers functions with growing  $Q^2$  and a simultaneous widening of its Gaussian width. It is interesting to point out that the analytical TMD approximation, for the Sivers function visibly breaks down for large values of  $k_{\perp}$ .

## II. SIDIS DATA AND TMD VERSUS NON-TMD EVOLUTION

Having established the phenomenological formalism necessary to implement the TMD evolution, as given in Refs. [7–9], we apply it to the Sivers function. This TMD distribution,  $\Delta^N \hat{f}_{q/p^i}(x, k_{\perp}, Q) = (-2k_{\perp}/M_p)\hat{f}_{1T}^{\perp}$ , can be extracted from HERMES and COMPASS  $\ell p \rightarrow hX$  SIDIS data on the azimuthal moment  $A_{UT}^{\sin(\phi_h - \phi_S)}$ , defined as

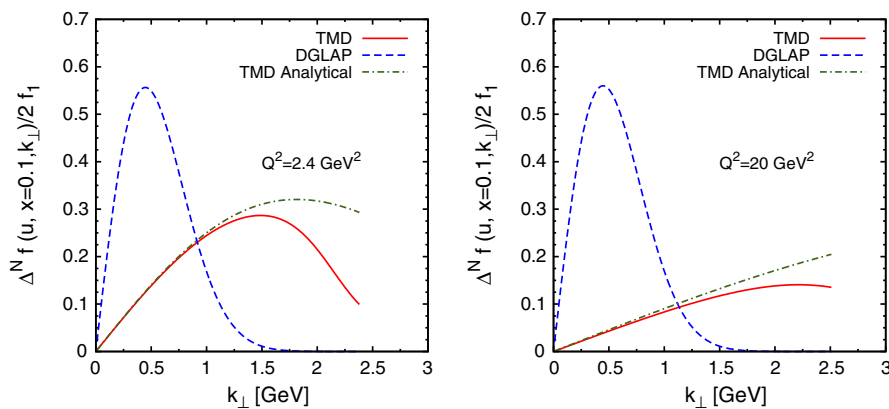


FIG. 3 (color online). The left panel shows the ratio Sivers/PDF,  $\Delta^N \hat{f}_{u/p^i}/2\hat{f}_{u/p}$ , evolved from the initial scale,  $Q_0^2 = 1 \text{ GeV}^2$ , to  $Q^2 = 2.4 \text{ GeV}^2$ , using TMD evolution (red, solid line), DGLAP evolution (blue, dashed line) and the analytical approximated TMD evolution (green, dot-dashed line). The right panel shows the same functions at the scale  $Q^2 = 20 \text{ GeV}^2$ . Notice that, while there is almost no difference between the DGLAP-evolved lines at  $Q^2 = 2.4$  and  $Q^2 = 20 \text{ GeV}^2$ , the TMD evolution induces a fast decrease in size of the ratio Sivers/PDF functions with growing  $Q^2$  and a simultaneous widening of its Gaussian width. It is interesting to point out that the analytical approximation, for the Sivers function, visibly breaks down at large values of  $k_{\perp}$ .

$$A_{UT}^{\sin(\phi_h - \phi_S)} = 2 \frac{\int d\phi_S d\phi_h [d\sigma^\uparrow - d\sigma^\downarrow] \sin(\phi_h - \phi_S)}{\int d\phi_S d\phi_h [d\sigma^\uparrow + d\sigma^\downarrow]}. \quad (34)$$

This transverse single spin asymmetry embeds the azimuthal modulation triggered by the correlation between the nucleon spin and the quark intrinsic transverse

momentum. The ‘‘weighting’’ factor  $\sin(\phi_h - \phi_S)$  in Eq. (34) is appropriately chosen to single out, among the various azimuthal dependent terms appearing in  $[d\sigma^\uparrow - d\sigma^\downarrow]$ , only the contribution of the Sivers mechanism [18,19]. By properly taking into account all intrinsic motions this transverse single spin asymmetry can be written as [1]

$$A_{UT}^{\sin(\phi_h - \phi_S)} = \frac{\sum_q \int d\phi_S d\phi_h d^2k_\perp \Delta^N \hat{f}_{q/p^i}(x, k_\perp, Q) \sin(\varphi - \phi_S) \frac{d\hat{\sigma}^{\ell q \rightarrow \ell q}}{dQ^2} \hat{D}_q^h(z, p_\perp, Q) \sin(\phi_h - \phi_S)}{\sum_q \int d\phi_S d\phi_h d^2k_\perp \hat{f}_{q/p}(x, k_\perp, Q) \frac{d\hat{\sigma}^{\ell q \rightarrow \ell q}}{dQ^2} \hat{D}_q^h(z, p_\perp, Q)}. \quad (35)$$

With respect to the leptonic plane,  $\phi_S$  and  $\phi_h$  are the azimuthal angles identifying the transverse directions of the proton spin  $\mathbf{S}$  and of the outgoing hadron  $h$  respectively, while  $\varphi$  defines the direction of the incoming (and outgoing) quark transverse momentum,  $\mathbf{k}_\perp = k_\perp(\cos\varphi, \sin\varphi, 0)$ ;  $d\hat{\sigma}^{\ell q \rightarrow \ell q}/dQ^2$  is the unpolarized cross section for the elementary scattering  $\ell q \rightarrow \ell q$ .

The aim of our paper is to analyze the available polarized SIDIS data from the HERMES and COMPASS Collaborations in order to understand whether or not they show signs of the TMD evolution proposed in Ref. [9] and described in Sec. IA. Our general strategy is that of adopting the TMD evolution in the extraction of the Sivers functions, with the same parametrization and input functions as in Refs. [5,13], and see if that can improve the quality of the fits. In doing so we will make use of the HERMES reanalysis of SIDIS experimental data on Sivers asymmetries for pion and kaon production and the newest SIDIS COMPASS data off a proton target, which cover a wider range of  $Q^2$  values, thus giving a better opportunity to check the TMD evolution.

In particular we perform three different data fits:

- (i) a fit (TMD fit) in which we adopt the TMD-evolution equation discussed in Secs. IA and IB, Eqs. (23)–(25) and (8)–(10);
- (ii) a second fit (TMD analytical fit) in which we apply the same TMD evolution, but using the analytical approximation discussed in Sec. IC, Eqs. (27), (30), and (32);
- (iii) a fit (DGLAP fit) in which we follow our previous work, as done so far in Ref. [5,13], using the DGLAP evolution equation only in the collinear part of the TMDs.

As a result of the fit we will have explicit expressions of all the Sivers functions and their parameters. However, the goal of the paper is not that of obtaining a new extraction of the Sivers distributions, although we will show, for comment and illustration purposes, the Sivers functions for  $u$  and  $d$  valence quarks, with the relative parameters. The procedure followed here aims at testing the effect of the TMD evolution, as compared with the simple DGLAP

evolution so far adopted, in fitting the TMD SIDIS data. If it turns out, as it will, that this improves the quality of the fit, then a new extraction of the Sivers distributions, entirely guided by the TMD evolution, will be necessary. That will require a different approach from the very beginning, with different input functions and parametrizations.

Here, we parametrize the Sivers function at the initial scale  $Q_0 = 1$  GeV, as in Ref. [5,13], in the following form:

$$\Delta^N \hat{f}_{q/p^i}(x, k_\perp, Q_0) = 2 \mathcal{N}_q(x) h(k_\perp) \hat{f}_{q/p}(x, k_\perp, Q_0), \quad (36)$$

with

$$\mathcal{N}_q(x) = N_q x^{\alpha_q} (1-x)^{\beta_q} \frac{(\alpha_q + \beta_q)^{(\alpha_q + \beta_q)}}{\alpha_q^{\alpha_q} \beta_q^{\beta_q}}, \quad (37)$$

$$h(k_\perp) = \sqrt{2} e^{-k_\perp^2/M_1^2}, \quad (38)$$

where  $\hat{f}_{q/p}(x, k_\perp, Q_0)$  is defined in Eq. (15) and  $N_q$ ,  $\alpha_q$ ,  $\beta_q$  and  $M_1$  (GeV) are (scale-independent) free parameters to be determined by fitting the experimental data. Since  $h(k_\perp) \leq 1$  for any  $k_\perp$  and  $|\mathcal{N}_q(x)| \leq 1$  for any  $x$  (notice that we allow the constant parameter  $N_q$  to vary only inside the range  $[-1, 1]$ ), the positivity bound for the Sivers function,

$$\frac{|\Delta^N \hat{f}_{q/p^i}(x, k_\perp)|}{2 \hat{f}_{q/p}(x, k_\perp)} \leq 1, \quad (39)$$

is automatically fulfilled. Similarly to PDFs, the FFs at the initial scale are parametrized with a Gaussian shape, Eq. (17).

As in Refs. [5,20], the average values of  $k_\perp$  and  $p_\perp$  are fixed as

$$\langle k_\perp^2 \rangle = 0.25 \text{ GeV}^2 \quad \langle p_\perp^2 \rangle = 0.20 \text{ GeV}^2. \quad (40)$$

We take the unpolarized distributions  $f_{q/p}(x, Q_0^2)$  from Ref. [21] and the unpolarized fragmentation functions  $D_{h/q}(z, Q_0^2)$  from Ref. [22], with  $Q_0^2 = 1.0$  GeV. As in Ref. [5], we adopt 11 free parameters,

TABLE I.  $\chi^2$  contributions corresponding to the TMD fit, the TMD analytical fit and the DGLAP fit, for each experimental data set of HERMES and COMPASS experiments.

| Experiment | Hadron  | N. points | TMD evolution (exact)   | TMD evolution (analytical)                                      | DGLAP evolution   |
|------------|---------|-----------|---|---|---|
|            |         |           | $\chi_{\text{tot}}^2 = 255.8$<br>$\chi_{\text{d.o.f}}^2 = 1.02$ | $\chi_{\text{tot}}^2 = 275.7$<br>$\chi_{\text{d.o.f}}^2 = 1.10$ | $\chi_{\text{tot}}^2 = 315.6$<br>$\chi_{\text{d.o.f}}^2 = 1.26$ |
| HERMES     | $\pi^+$ | 7         | $\chi_x^2 = 10.7$   | $\chi_x^2 = 12.9$   | $\chi_x^2 = 27.5$   |
|            |         | 7         | $\chi_z^2 = 4.3$  | $\chi_z^2 = 4.3$  | $\chi_z^2 = 8.6$  |
|            |         | 7         | $\chi_{P_T}^2 = 9.1$  | $\chi_{P_T}^2 = 10.5$   | $\chi_{P_T}^2 = 22.5$   |
|            | $\pi^-$ | 7         | $\chi_x^2 = 17.0$   | $\chi_x^2 = 16.5$   | $\chi_x^2 = 14.8$   |
|            |         | 7         | $\chi_z^2 = 2.4$  | $\chi_z^2 = 2.4$  | $\chi_z^2 = 3.3$  |
|            |         | 7         | $\chi_{P_T}^2 = 6.4$  | $\chi_{P_T}^2 = 6.3$  | $\chi_{P_T}^2 = 6.2$  |
|            | $\pi^0$ | 7         | $\chi_x^2 = 5.9$  | $\chi_x^2 = 5.8$  | $\chi_x^2 = 5.6$  |
|            |         | 7         | $\chi_z^2 = 8.0$  | $\chi_z^2 = 8.1$  | $\chi_z^2 = 6.9$  |
|            |         | 7         | $\chi_{P_T}^2 = 6.8$  | $\chi_{P_T}^2 = 7.0$  | $\chi_{P_T}^2 = 6.6$  |
|            | $K^+$   | 7         | $\chi_x^2 = 4.7$  | $\chi_x^2 = 4.8$  | $\chi_x^2 = 4.4$  |
|            |         | 7         | $\chi_z^2 = 9.3$  | $\chi_z^2 = 9.8$  | $\chi_z^2 = 4.3$  |
|            |         | 7         | $\chi_{P_T}^2 = 4.6$  | $\chi_{P_T}^2 = 5.3$  | $\chi_{P_T}^2 = 2.8$  |
|            | $K^-$   | 7         | $\chi_x^2 = 2.4$  | $\chi_x^2 = 2.4$  | $\chi_x^2 = 2.9$  |
|            |         | 7         | $\chi_z^2 = 7.2$  | $\chi_z^2 = 7.0$  | $\chi_z^2 = 5.5$  |
|            |         | 7         | $\chi_{P_T}^2 = 3.4$  | $\chi_{P_T}^2 = 3.3$  | $\chi_{P_T}^2 = 3.7$  |
| COMPASS-p  | $h^+$   | 9         | $\chi_x^2 = 6.7$  | $\chi_x^2 = 11.2$   | $\chi_x^2 = 29.2$   |
|            |         | 8         | $\chi_z^2 = 17.8$   | $\chi_z^2 = 18.5$   | $\chi_z^2 = 16.6$   |
|            |         | 9         | $\chi_{P_T}^2 = 12.4$   | $\chi_{P_T}^2 = 24.2$   | $\chi_{P_T}^2 = 11.8$   |
|            | $h^-$   | 9         | $\chi_x^2 = 7.6$  | $\chi_x^2 = 7.7$  | $\chi_x^2 = 11.9$   |
|            |         | 8         | $\chi_z^2 = 9.7$  | $\chi_z^2 = 9.6$  | $\chi_z^2 = 14.1$   |
|            |         | 9         | $\chi_{P_T}^2 = 8.1$  | $\chi_{P_T}^2 = 8.1$  | $\chi_{P_T}^2 = 9.9$  |
| COMPASS-d  | $\pi^+$ | 9         | $\chi_x^2 = 7.3$  | $\chi_x^2 = 7.1$  | $\chi_x^2 = 5.3$  |
|            |         | 8         | $\chi_z^2 = 5.4$  | $\chi_z^2 = 5.3$  | $\chi_z^2 = 7.9$  |
|            |         | 9         | $\chi_{P_T}^2 = 5.4$  | $\chi_{P_T}^2 = 5.2$  | $\chi_{P_T}^2 = 5.5$  |
|            | $\pi^-$ | 9         | $\chi_x^2 = 4.4$  | $\chi_x^2 = 4.4$  | $\chi_x^2 = 5.0$  |
|            |         | 8         | $\chi_z^2 = 10.9$   | $\chi_z^2 = 10.7$   | $\chi_z^2 = 13.9$   |
|            |         | 9         | $\chi_{P_T}^2 = 4.5$  | $\chi_{P_T}^2 = 4.8$  | $\chi_{P_T}^2 = 4.4$  |
|            | $K^+$   | 9         | $\chi_x^2 = 6.5$  | $\chi_x^2 = 6.5$  | $\chi_x^2 = 5.8$  |
|            |         | 8         | $\chi_z^2 = 7.7$  | $\chi_z^2 = 7.7$  | $\chi_z^2 = 7.2$  |
|            |         | 9         | $\chi_{P_T}^2 = 4.8$  | $\chi_{P_T}^2 = 4.9$  | $\chi_{P_T}^2 = 4.7$  |
|            | $K^-$   | 9         | $\chi_x^2 = 12.1$   | $\chi_x^2 = 12.4$   | $\chi_x^2 = 13.1$   |
|            |         | 8         | $\chi_z^2 = 8.9$  | $\chi_z^2 = 9.0$  | $\chi_z^2 = 9.4$  |
|            |         | 9         | $\chi_{P_T}^2 = 13.5$   | $\chi_{P_T}^2 = 12.0$   | $\chi_{P_T}^2 = 14.4$   |

TABLE II. Best values of the free parameters, Eq. (41), for the Sivers functions of  $u$  and  $d$  valence quarks, as obtained from our TMD fit, TMD analytical fit and DGLAP fit, at  $Q_0 = 1$  GeV. The errors reported in this table correspond to the maximum and minimum values of each parameter in a restricted parameter space constrained by the condition  $\Delta\chi^2 = 20$ , corresponding to 95.45% confidence level. They correspond to the shaded area in Fig. 7.

| TMD evolution (exact)                          | TMD evolution (analytical)                      | DGLAP evolution                                 |
|--|---|---|
| $N_{u_v} = 0.77^{+0.23}_{-0.19}$               | $N_{u_v} = 0.75^{+0.25}_{-0.21}$                | $N_{u_v} = 0.45^{+0.25}_{-0.17}$                |
| $N_{d_v} = -1.00^{+0.75}_{-0.00}$              | $N_{d_v} = -1.00^{+0.82}_{-0.00}$               | $N_{d_v} = -1.00^{+0.85}_{-0.00}$               |
| $\alpha_{u_v} = 0.68^{+0.57}_{-0.40}$          | $\alpha_{u_v} = 0.82^{+0.51}_{-0.48}$           | $\alpha_{u_v} = 1.08^{+0.68}_{-0.62}$           |
| $\alpha_{d_v} = 1.11^{+1.39}_{-0.91}$          | $\alpha_{d_v} = 1.36^{+1.24}_{-1.00}$           | $\alpha_{d_v} = 1.7^{+1.15}_{-0.91}$            |
| $\beta = 3.1^{+4.7}_{-2.6}$                    | $\beta = 4.0^{+4.5}_{-2.8}$                     | $\beta = 6.9^{+6.4}_{-4.1}$                     |
| $M_1^2 = 0.40^{+1.5}_{-0.23}$ GeV <sup>2</sup> | $M_1^2 = 0.34^{+1.36}_{-0.19}$ GeV <sup>2</sup> | $M_1^2 = 0.19^{+0.77}_{-0.10}$ GeV <sup>2</sup> |

$$\begin{array}{cccccc}
 N_{u_v} & N_{d_v} & N_s & N_{\bar{u}} & N_{\bar{d}} & N_{\bar{s}} \\
 \alpha_{u_v} & \alpha_{d_v} & \alpha_{\text{sea}} & \beta & M_1(\text{GeV}) & 
 \end{array} \quad (41)$$

where the subscript  $v$  denotes valence contributions. In this choice we differ from Ref. [5], where valence and sea contributions were not separated.

We perform best fits of 11 experimental data sets: HERMES [11] data for SIDIS production of pions ( $\pi^+$ ,  $\pi^-$ ,  $\pi^0$ ) and kaons ( $K^+$  and  $K^-$ ), COMPASS data for SIDIS pion ( $\pi^+$ ,  $\pi^-$ ) and kaon ( $K^+$  and  $K^-$ ) production from a LiD (deuteron) target [23], and the preliminary COMPASS data for charged hadron production from an  $\text{NH}_3$  (proton) target [12]. The results of these three fits are presented in Table I in terms of their  $\chi^2$ s.

As is clear from the first line of Table I, the best total  $\chi^2_{\text{tot}}$ , which amounts to 256, is obtained by using the TMD evolution, followed by a slightly higher  $\chi^2_{\text{tot}}$  of the analytical

approximation, and a definitely larger  $\chi^2_{\text{tot}} \simeq 316$  corresponding to the DGLAP fit. To examine the origin of this difference between TMD and DGLAP evolution, we show the individual contributions to  $\chi^2_{\text{tot}}$  of each experiment (HERMES, COMPASS on  $\text{NH}_3$  and on  $\text{LiD}$  targets), for all types of detected hadrons and for all variables observed ( $x$ ,  $z$  and  $P_T$ ). A global look at the numbers reported in Table I shows that the difference of about 60  $\chi^2$  points between the TMD and the DGLAP fits is not equally distributed among all  $\chi^2$ s per data point; rather, it is heavily concentrated in three particular cases, namely in the asymmetry for  $\pi^+$  production at HERMES and for  $h^+$  and  $h^-$  production at COMPASS off a proton target, especially when this asymmetry is observed as a function of the  $x$  variable.

It is important to stress that, as  $x$  is directly proportional to  $Q^2$  through the kinematical relation  $Q^2 = xys$ , the  $x$  behavior of the asymmetries is intimately connected to their  $Q^2$  evolution. While the HERMES experimental

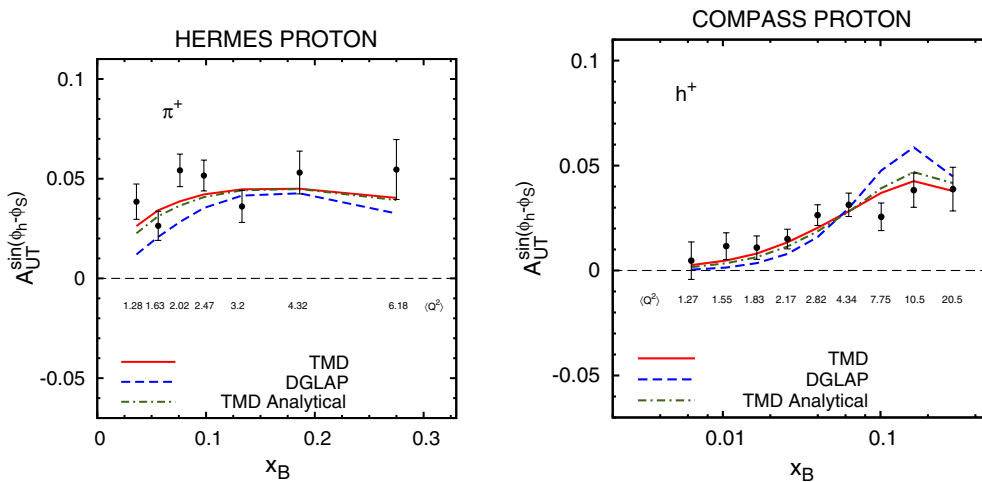


FIG. 4 (color online). The results obtained from our fit of the SIDIS  $A_{UT}^{\sin(\phi_h - \phi_s)}$  Sivers asymmetries applying TMD evolution (red, solid lines) are compared with the analogous results found by using DGLAP-evolution equations (blue, dashed lines). The green, dash-dotted lines correspond to the results obtained by using the approximated analytical TMD evolution (see text for further details). The experimental data are from HERMES [11] (left panel) and COMPASS [12] (right panel) Collaborations.

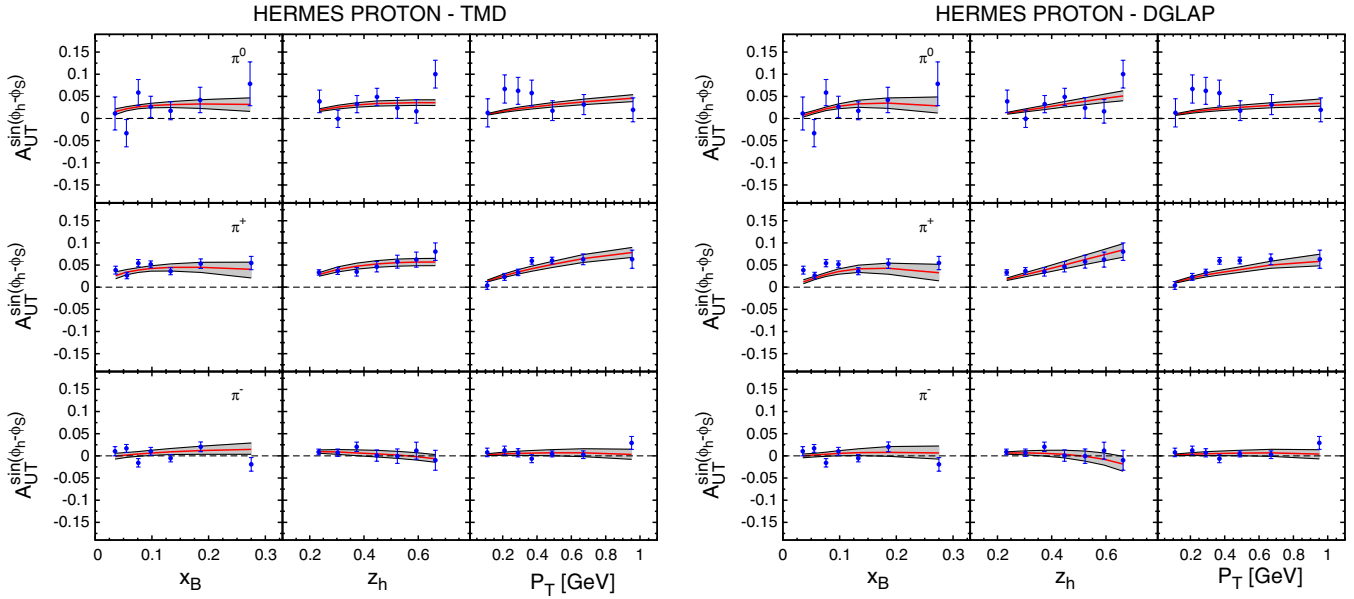


FIG. 5 (color online). The results obtained from the TMD-evolution fit (left panel) and from the DGLAP-evolution fit (right panel) of the SIDIS  $A_{UT}^{\sin(\phi_h - \phi_s)}$  Sivers asymmetries (red, solid lines) are compared with the HERMES experimental data [11] for charged and neutral pion production. The shaded area corresponds to the statistical uncertainty of the parameters, see Appendix A of Ref. [5] for further details.

bins cover a very modest range of  $Q^2$  values, from  $1.3 \text{ GeV}^2$  to  $6.2 \text{ GeV}^2$ , COMPASS data raise to a maximum  $Q^2$  of  $20.5 \text{ GeV}^2$ , enabling to test more severely the TMD  $Q^2$  evolution in SIDIS.

These aspects are illustrated in Fig. 4, where the SIDIS Sivers asymmetries  $A_{UT}^{\sin(\phi_h - \phi_s)}$  obtained in the 3 fits are shown in the same plot. It is evident that the DGLAP evolution seems to be unable to describe the correct  $x$  trend, i.e., the right  $Q^2$  behavior, while the TMD evolution (red, solid line) follows much better the large  $Q^2$  data points, corresponding to the last  $x$  bins measured by COMPASS. The approximate

analytical TMD evolution (green, dash-dotted line) works very well for low to moderate values of  $Q^2$  while it starts to deviate from the exact behavior at large  $Q^2$  values.

In Figs. 5 we show, as an illustration of their qualities, our best fits (red, solid lines) of the HERMES experimental data [11] on the Sivers asymmetries for pion production. Those on the left panels are obtained adopting the new TMD evolution, while those on the right use the simplified DGLAP evolution. Similar results are shown, for the recent COMPASS data off a proton target [12] for charged hadron production, in Fig. 6.

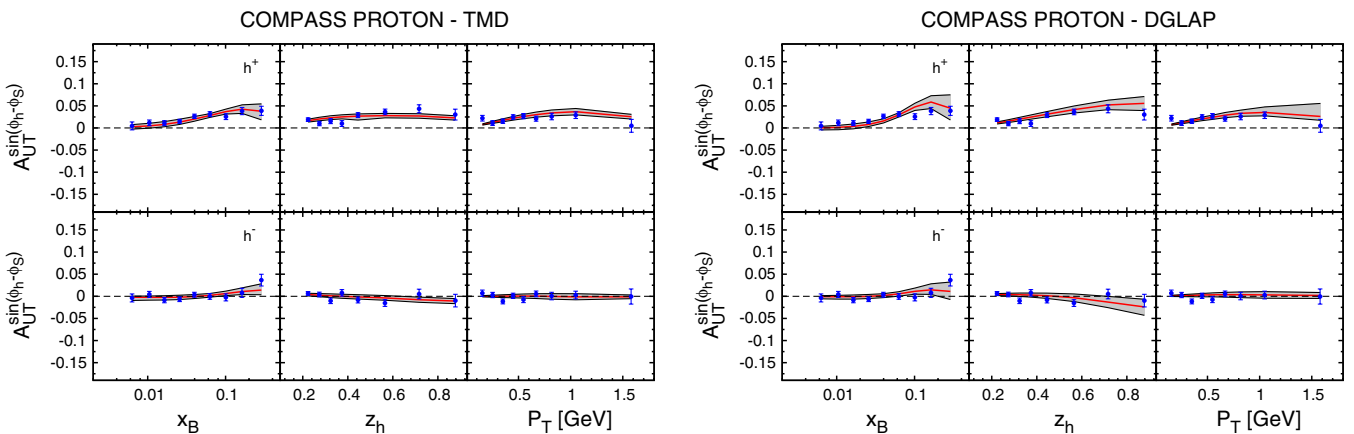


FIG. 6 (color online). The results obtained from the TMD-evolution fit (left panel) and from the DGLAP-evolution fit (right panel) of the SIDIS  $A_{UT}^{\sin(\phi_h - \phi_s)}$  Sivers asymmetries (red, solid lines) are compared with the COMPASS-p experimental data [12] for charged hadron production. The shaded area corresponds to the statistical uncertainty of the parameters, see Appendix A of Ref. [5] for further details.

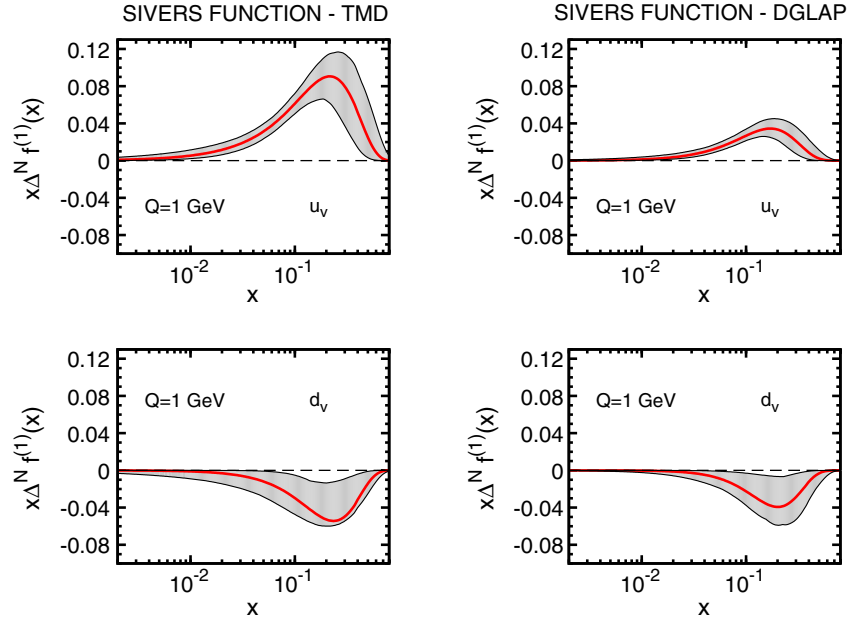


FIG. 7 (color online). The first moment of the valence  $u$  and  $d$  Sivers functions, evaluated at  $Q = Q_0$ , obtained from our best fits of the  $A_{UT}^{\sin(\phi_h - \phi_s)}$  azimuthal moments as measured by HERMES [11] and COMPASS [12,23] Collaborations. The extraction of the Sivers functions on the left side takes into account the TMD evolution (left column of Table II), while for those on the right side it does not (right column of Table II). The shaded area corresponds to the statistical uncertainty of the parameters, see Appendix A of Ref. [5] for further details.

The shaded area represents the statistical uncertainty of the fit parameters corresponding to a  $\Delta\chi^2 = 20$  (i.e.) to 95.45% confidence level for 11 degrees of freedom, see Appendix A of Ref. [5] for further details). Notice that, in general, the error bands corresponding to the TMD evolution fit are thinner than those corresponding to the DGLAP fit: this is caused by the fact that the TMD evolution implies a ratio Sivers/PDF which becomes smaller with growing  $Q^2$ , as shown in Fig. 3, constraining the free parameters much more tightly than in the DGLAP evolution fit, where the Sivers/PDF ratio remains roughly constant as  $Q^2$  raises from low to large values.

In Fig. 7 we compare, for illustration purposes, the Sivers function—actually, its first moment, defined in Ref. [5]—at the initial scale  $Q_0$  for  $u$  and  $d$  valence quarks, as obtained in our best fits with the TMD (left panel) and the DGLAP (right panel) evolution, Table II. Notice that for this analysis we have chosen to separate valence from sea quark contributions, while in Ref. [5] the  $u$  and  $d$  flavors included all contributions.

This result deserves some comments. The comparison shows that the extracted  $u$  and  $d$  valence contributions, at the initial scale  $Q_0 = 1$  GeV, are definitely larger for the TMD-evolution fit. This reflects the TMD-evolution property, according to which the Sivers functions are strongly suppressed with increasing  $Q^2$ , which is not the case for the almost static collinear DGLAP evolution. Thus, in order to fit the same data at  $Q^2$  bins ranging from 1.3 to 20.5 GeV<sup>2</sup>, the TMD-evolving Sivers functions must start from higher values at  $Q_0 = 1$  GeV. The Sivers distributions previously

extracted, with the DGLAP evolution, in Refs. [5,13] were given at  $Q^2 = 2.4$  GeV<sup>2</sup>; one should notice that if we TMD evolve the Sivers distributions on the left side of Fig. 7 up to  $Q^2 = 2.4$  GeV<sup>2</sup> we would obtain a result very close to that of Refs. [5,13] (and to that of the right side of Fig. 7).

### III. CONCLUSIONS AND FURTHER REMARKS

We have addressed the issue of testing whether or not the recently proposed  $Q^2$  evolution of the TMDs (TMD evolution) can already be observed in the available SIDIS data on the Sivers asymmetry. It is a first crucial step towards the implementation, based on the TMD-evolution equations of Refs. [7–9], of a consistent QCD framework in which to study the TMDs and their full  $Q^2$  dependence. That would put the study of TMDs—and the related reconstruction of the three-dimensional parton momentum structure of the nucleons—on a firm basis, comparable to that used for the integrated PDFs.

Previous extractions of the Sivers functions from SIDIS data included some simplified treatment of the  $Q^2$  evolution, which essentially amounted to consider the evolution of the collinear and factorized part of the distribution and fragmentation functions (DGLAP evolution). It induced modest effects, because of the slow  $Q^2$  evolution and of the limited  $Q^2$  range spanned by the available data. The situation has recently much progressed, for two reasons: the new TMD evolution [8,9] shows a strong variation with  $Q^2$  of the functional form

of the unpolarized and Sivers TMDs, as functions of the intrinsic momentum  $k_{\perp}$ ; in addition, some new COMPASS results give access to Sivers asymmetries at larger  $Q^2$  values.

It appears then possible to test the new TMD evolution. In order to do so one has to implement the full machinery of the TMD-evolution equations in a viable phenomenological scheme. We have done so, following Ref. [9], and the simplified version of the TMD evolution given in Eqs. (6) and (7). We have used them in our previous procedure adopted for the extraction of the Sivers functions [5,13,18], with the same input parameters; moreover, we have considered also the updated HERMES [11] and the new COMPASS [12] data.

A definite statement resulting from our analysis is that the best fit of all SIDIS data on the Sivers asymmetry using TMD evolution, when compared with the same analysis performed with the simplified DGLAP evolution, exhibits a smaller value of the total  $\chi^2$ , as shown in Table I. Not only, but when analyzing the partial contributions to the total  $\chi^2$  value of the single subsets of data, one realizes that such a smaller value mostly originates from the large  $Q^2$  COMPASS data, which are greatly affected by the TMD evolution. We consider this as an indication in favor of the TMD evolution.

A more comprehensive study of the TMD evolution and its phenomenological implications is now necessary. Both the general scheme and its application to physical processes need improvements. The recovery of the usual collinear DGLAP evolution equations, after integration of the TMD evolution results over the intrinsic momenta, has to be understood. Consider, as an example, the simple expression of the evolution of the unpolarized TMD PDF, as given in Eq. (27). Such an evolution describes how the TMD dependence on  $k_{\perp}$  changes with  $Q^2$ , but does not induce any change in the  $x$  dependence, which, at this order, remains fixed and factorized. The question whether or not one can recover the usual DGLAP evolution, which changes the  $x$  dependence, for the integrated PDFs arises naturally at this point. A naive integration of Eq. (27) on  $k_{\perp}$ , over the full integration range, would give  $f_{q/p}(x, Q) = f_{q/p}(x, Q_0)R(Q, Q_0)$  which is not the correct PDF evolution. However, the  $k_{\perp}$  integration should have upper limits which depend on  $x$  and  $Q^2$ , and the full TMD evolution is more complicated than the simplified version

used here, as explained at the beginning of Sec. IA. These issues were also recently addressed, within a soft-collinear effective theory framework, in Ref. [24].

We have made a safe phenomenological use of the TMD-evolution equations; it is true that they induce a strong change in the  $k_{\perp}$  dependence of the unpolarized and Sivers TMDs, leaving unchanged the  $x$ -dependent shape, thus neglecting the collinear DGLAP evolution, but this should not be a problem. In fact, as we have shown explicitly in Fig. 2 (dashed curve), the collinear DGLAP evolution is negligible in the  $Q^2$  region considered; Fig. 2 is drawn for  $x = 0.1$ , but a similar conclusion holds for all  $x$  values involved in the SIDIS data used in the paper. Moreover, the extra factors  $R(Q, Q_0)$ , arising in the TMD evolution, cancel out, as already explained, in the expression of the Sivers asymmetries.

Further help to the study of the TMD evolution of the Sivers function, valid at larger  $k_{\perp}$  values, might possibly come from its evolution written in terms of the twist-3 Efremov-Teryaev-Qiu-Sterman function  $T_{q,F}$ , as in Eq. (47) of Ref. [9]; this function is related to the first  $k_{\perp}$ -moment of the quark Sivers function [25]. An extraction of  $T_{q,F}$ , from data on single spin asymmetries in single inclusive large  $P_T$  hadron production in  $pp$  collisions, is available in the literature [26]. However, a “sign-mismatch” problem [27] between the twist-3 function from  $pp$  data and the Sivers function from SIDIS data has recently been pointed out, and we do not pursue this point further.

A fresh analysis of TMD-dependent data, both in polarized and unpolarized, SIDIS and Drell-Yan processes, has to be carefully performed including TMD evolution from the beginning in an unbiased way. Most importantly so, should predictions for future high-energy experiments, like the planned electron-ion/electron-nucleon colliders, be considered or reconsidered.

## ACKNOWLEDGMENTS

We thank Umberto D’Alesio, Francesco Murgia and Alexei Prokudin for interesting and fruitful discussions. We acknowledge support of the European Community under the FP7 “Capacities-Research Infrastructures” program (HadronPhysics3, Grant Agreement No. 283286). We acknowledge partial support by MIUR under Cofinanziamento PRIN 2008.

- 
- [1] M. Anselmino, M. Boglione, U. D’Alesio, A. Kotzinian, F. Murgia, and A. Prokudin, *Phys. Rev. D* **72**, 094007 (2005); **72**, 099903(E) (2005).
- [2] J.C. Collins, A.V. Efremov, K. Goeke, S. Menzel, A. Metz, and P. Schweitzer, *Phys. Rev. D* **73**, 014021 (2006).

- [3] W. Vogelsang and F. Yuan, *Phys. Rev. D* **72**, 054028 (2005).
- [4] M. Anselmino *et al.*, in *Proceedings of the International Workshop on Transverse Polarisation Phenomena in Hard Processes (Transversity 2005, Como, Italy)* (World Scientific, Singapore, 2005).

- [5] M. Anselmino, M. Boglione, U. D'Alesio, A. Kotzinian, S. Melis, F. Murgia, A. Prokudin, and C. Türk, *Eur. Phys. J. A* **39**, 89 (2008).
- [6] A. Bacchetta and M. Radici, *Phys. Rev. Lett.* **107**, 212001 (2011).
- [7] J.C. Collins, *Foundations of Perturbative QCD*, Cambridge Monographs on Particle Physics, Nuclear Physics and Cosmology Vol. 32 (Cambridge University Press, Cambridge, 2011).
- [8] S.M. Aybat and T.C. Rogers, *Phys. Rev. D* **83**, 114042 (2011).
- [9] S.M. Aybat, J.C. Collins, J.-W. Qiu, and T.C. Rogers, *Phys. Rev. D* **85**, 034043 (2012).
- [10] S.M. Aybat, A. Prokudin, and T.C. Rogers, [arXiv:1112.4423](https://arxiv.org/abs/1112.4423).
- [11] A. Airapetian *et al.* (HERMES Collaboration), *Phys. Rev. Lett.* **103**, 152002 (2009).
- [12] F. Bradamante (COMPASS Collaboration), [arXiv:1111.0869](https://arxiv.org/abs/1111.0869).
- [13] M. Anselmino, M. Boglione, U. D'Alesio, S. Melis, F. Murgia, and A. Prokudin, [arXiv:1107.4446](https://arxiv.org/abs/1107.4446).
- [14] J.C. Collins and D.E. Soper, *Nucl. Phys.* **B197**, 446 (1982).
- [15] J.C. Collins, D.E. Soper, and G.F. Sterman, *Nucl. Phys.* **B250**, 199 (1985).
- [16] D. Sivers, *Phys. Rev. D* **41**, 83 (1990); **43**, 261 (1991).
- [17] F. Landry, R. Brock, P.M. Nadolsky, and C.-P. Yuan, *Phys. Rev. D* **67**, 073016 (2003).
- [18] M. Anselmino, M. Boglione, U. D'Alesio, S. Melis, F. Murgia, E.R. Nocera, and A. Prokudin, *Phys. Rev. D* **83**, 114019 (2011).
- [19] A. Bacchetta, M. Diehl, K. Goetze, A. Metz, P.J. Mulders, and M. Schlegel, *J. High Energy Phys.* **02** (2007) 093.
- [20] M. Anselmino, M. Boglione, U. D'Alesio, A. Kotzinian, F. Murgia, and A. Prokudin, *Phys. Rev. D* **71**, 074006 (2005).
- [21] M. Gluck, E. Reya, and A. Vogt, *Eur. Phys. J. C* **5**, 461 (1998).
- [22] D. de Florian, R. Sassot, and M. Stratmann, *Phys. Rev. D* **75**, 114010 (2007).
- [23] M. Alekseev *et al.* (COMPASS Collaboration), *Phys. Lett. B* **673**, 127 (2009).
- [24] M. Garcia-Echevarria, A. Idilbi, and I. Scimemi, [arXiv:1111.4996](https://arxiv.org/abs/1111.4996).
- [25] D. Boer, P.J. Mulders, and F. Pijlman, *Nucl. Phys.* **B667**, 201 (2003).
- [26] C. Kouvaris, J.-W. Qiu, W. Vogelsang, and F. Yuan, *Phys. Rev. D* **74**, 114013 (2006).
- [27] Z.-B. Kang, J.-W. Qiu, W. Vogelsang, and F. Yuan, *Phys. Rev. D* **83**, 094001 (2011).